Spin-Orbit-Coupled Bose-Einstein Condensates in a One-Dimensional Optical Lattice

C. Hamner,[1] Yongping Zhang,[2,3] M. A. Khamehchi,[1] Matthew J. Davis,[2] and P. Engels[1,*]

[1]*Department of Physics and Astronomy, Washington State University, Pullman, Washington 99164, USA*
[2]*The University of Queensland, School of Mathematics and Physics, St Lucia, Queensland 4072, Australia*
[3]*Quantum Systems Unit, OIST Graduate University, Onna, Okinawa 904-0495, Japan*

We investigate a spin-orbit-coupled Bose-Einstein condensate loaded into a translating optical lattice. We experimentally demonstrate the lack of Galilean invariance in the spin-orbit-coupled system, which leads to anisotropic behavior of the condensate depending on the direction of translation of the lattice. The anisotropy is theoretically understood by an effective dispersion relation. We experimentally confirm this theoretical picture by probing the dynamical instability of the system.

Spin-orbit coupling (SOC), the interaction between a particle's spin and its mechanical motion, plays a prominent role in condensed matter physics [1]. Even though the spin-orbit interaction is usually relatively weak, it can be important for bands close to the Fermi level [2]. The combination of spin-orbit coupling with a periodic potential resulted in the prediction and discovery of topological insulators [3,4], which have become a significant focus of recent research [5,6]. Such spin-orbit-coupled lattice systems, with the addition of strongly correlated many-body effects, afford the possibility of studying new phase transitions and realizing exotic spin models [7,8].

In cold atomic gases, spin-orbit coupling can be implemented by Raman coupling of atomic hyperfine states [9–14]. The tunability of the Raman coupling parameters results in a flexible experimental platform to explore spin-orbit-coupled physics [15–18]. The spin-orbit coupling can strongly modify the single-particle dispersion relation of a quantum gas. The resulting novel band structures [9,19] give rise to many interesting phenomena due to the competition between spin-orbit coupling and atomic interactions (for recent reviews see, e.g., [20,21]).

In this Letter, we perform a detailed study of a Bose-Einstein condensate (BEC) with spin-orbit coupling loaded into a shallow one-dimensional optical lattice.

The effects of a stationary lattice can be understood by repeatedly displacing the single-particle SOC spectrum along the momentum axis by integer multiples of the reciprocal lattice vector. Where lines of displaced spectra cross, gaps open up. The resulting Bloch spectrum shows interesting features. For example, in a certain parameter regime, the lowest Bloch band can be flat [22]. If the lattice moves, the Bloch spectrum becomes complicated due to the lack of Galilean invariance in the presence of the spin-orbit coupling [23]. We develop an effective dispersion relation to depict the joint effect of spin-orbit coupling and the translating lattice. The breaking of Galilean invariance is naturally incorporated in the effective dispersion by its asymmetry with respect to different directions of motion.

The effective dispersion is probed experimentally by the observation of the dynamical instability of the condensate. The weak repulsive atomic interactions not only move the single-particle effective dispersion slightly upward [24], but also cause dynamical instability of certain Bloch states. A homogenous single component BEC with repulsive interactions is always dynamically stable. However, when loaded into an optical lattice, the BEC features dynamical instabilities when the speed of the translating lattice is larger than a critical value [25–28]. The instabilities are characterized by an initial exponential growth of excitations in the BEC, heating, and ultimately, loss of atoms from the BEC. They are most significant in the vicinity of a band gap, which provides a mechanism to probe the band gap structure in an experiment. In our spin-orbit-coupled lattice BEC, we characterize the strengths of the instabilities by the loss rate of condensate atoms and find that the strengths depend on both the lattice speed and direction of motion. The regimes with most significant instability are used to identify band gaps present in the effective dispersion. The directional dependence of the instabilities corroborates the asymmetry of the effective dispersion. Our experiments provide a direct observation of the lack of Galilean invariance in the spin-orbit-coupled systems [23,29]. We compare our results with a Bogoliubov analysis and find good agreement.

We begin by providing a brief description of our experimental system. Spin-orbit coupling in BECs can be induced by Raman dressing schemes [9–14], and the geometry of our experiment is shown schematically in Fig. 1(a). The Raman lasers couple the $|1, -1\rangle = |\downarrow\rangle$ and $|1, 0\rangle = |\uparrow\rangle$ states of a ^{87}Rb BEC in the $F = 1$ hyperfine manifold. A 10 G bias magnetic field causes a sufficiently large quadratic Zeeman splitting such that the $|1, +1\rangle$ state is far from resonance. Hence, the system realizes an effective spin-1/2 system [30]. The system without the one-dimensional lattice is modeled by the single-particle Hamiltonian $H_{\text{SOC}} = p_z^2/2m + \gamma p_z \sigma_z + \hbar \delta \sigma_z/2 + \hbar \Omega \sigma_x/2$ [9]. Here m is the atomic mass and $\{\sigma_i\}$ are the Pauli

matrices. The spin-orbit coupling strength is $\gamma = \hbar k_{\mathrm{Ram}}/m$, where k_{Ram} is the wave vector of the Raman beams projected onto the z direction, $k_{\mathrm{Ram}} = 2\pi/(\lambda_{\mathrm{Ram}}\sqrt{2})$ with $\lambda_{\mathrm{Ram}} \approx 789$ nm. δ is the detuning, and Ω is the Rabi frequency. A typical band structure for our parameters is shown in Fig. 1(c), where the band energies are

$$E_{\pm}(k_z) = (\hbar^2 k_z^2/2m) \pm \hbar\sqrt{[\gamma k_z + (\delta/2)]^2 + (\Omega^2/4)}.$$

Here, $\hbar k_z$ is the quasimomentum in the spin-orbit direction.

Two additional laser beams with $\lambda_{\mathrm{lat}} \approx 1540$ nm and small frequency difference $\Delta\nu$ generate the translating optical lattice. The lattice beams are collinear with the Raman lasers such that $k_{\mathrm{lat}} = 2\pi/(\lambda_{\mathrm{lat}}\sqrt{2})$. The single-particle Hamiltonian
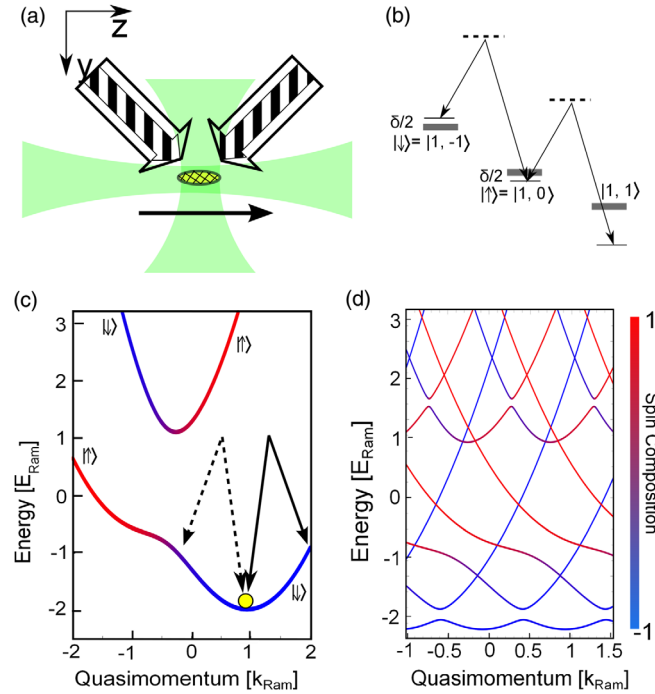

FIG. 1 (color online). Spin-orbit-coupled ^{87}Rb BEC in a one-dimensional optical lattice. (a) Experimental geometry. The BEC (yellow hashed) is confined in an optical dipole trap (solid green). Two sets of laser beams intersect the BEC at a 45° angle, generating the spin-orbit coupling (white arrow) and a translating optical lattice (striped arrows). (b) Raman coupling scheme in the $F = 1$ manifold of ^{87}Rb with detuning δ. (c) Typical band structure $E_{\pm}(k_z)$ of H_{SOC} with the color (gray scale) indicating the spin polarization, defined as the relative population difference of the bare spin components $(|\psi_{\uparrow}|^2 - |\psi_{\downarrow}|^2)/(|\psi_{\uparrow}|^2 + |\psi_{\downarrow}|^2)$. The BEC is prepared at the minimum of the lower band (circle). The arrows indicate a possible two-photon coupling due to the lattice translating with negative (dashed) or positive (solid) velocity. (d) Bloch spectrum of a stationary optical lattice in the presence of spin-orbit coupling. The lines correspond to $E_{\pm}(k_z)$ and $E_{\pm}(k_z + 2nk_{\mathrm{lat}})$, where n is an integer. The spin composition is encoded in the line color (gray scale). The parameters used for (c) and (d) are $\hbar\delta = 1.6E_{\mathrm{Ram}}$, $\hbar\Omega = 2E_{\mathrm{Ram}}$ with the additional parameters $U_0 = -1.4E_{\mathrm{lat}}$ and $v = 0$ for (d).

of the spin-orbit-coupled lattice system is $H_{\mathrm{sp}} = H_{\mathrm{SOC}} + U_0 \sin^2[k_{\mathrm{lat}}(z - vt)]$. The lattice velocity $v = \pi\Delta\nu/k_{\mathrm{lat}}$ can be adjusted by varying the frequency difference $\Delta\nu$ between the two lattice beams. For the experiments presented in this Letter, $U_0 = -1.4E_{\mathrm{lat}}$, where $E_{\mathrm{lat}} = \hbar^2 k_{\mathrm{lat}}^2/2m$. The presence of the optical lattice extends the spin-orbit-coupled bands in Fig. 1(c) to the Bloch spectrum in Fig. 1(d). In the repeated zone scheme, the Bloch spectrum is constructed through copies of the spin-orbit bands shifted by integers of the reciprocal lattice vector $2n\hbar k_{\mathrm{lat}}$ in quasimomentum and $2n\hbar k_{\mathrm{lat}}v$ in energy, where $n = 0, \pm1, \pm2, \ldots$. Gaps open in the Bloch spectrum wherever intersections between $E_{\pm}(k_z)$ and $E_{\pm}(k_z + 2nk_{\mathrm{lat}}) - 2n\hbar k_{lat}v$ occur. The width of the gap depends on the lattice depth U_0 and on the overlap between the spin composition of the states coupled by the lattice beams. Typically, the gap corresponding to $|n|$ is larger than that corresponding to $|n| + 1$. This is evident in Fig. 1(d), where the energy gaps are largest for $|n| = 1$ in both the lower as well as the upper dressed bands. Physically, the band gaps can be understood from multiphoton resonances in which the momentum of the atoms can be changed coherently by multiples of the reciprocal lattice vector $2n\hbar k_{\mathrm{lat}}$.

Before describing the experimental results, it is instructive to introduce an effective band structure picture. As the translating optical lattice potential is time dependent in the lab frame, it is convenient to go into the frame in which the optical lattice is stationary. This results in the Hamiltonian $H_{\mathrm{sp}}^M = p_z^2/2m + \gamma p_z \sigma_z + (\hbar\delta/2)\sigma_z + U_0\sin^2(k_{\mathrm{lat}}z) - vp_z$. With a simple substitution, $P = p_z - mv$, one obtains $\bar{H}_{\mathrm{sp}}^M = P^2/2m + \gamma P\sigma_z + (\delta + 2m\gamma v/\hbar)(\hbar/2)\sigma_z + (\hbar\Omega/2)\sigma_x + U_0\sin^2(k_{\mathrm{lat}}z)$ (where we have left out a constant energy term $mv^2/2$). In addition
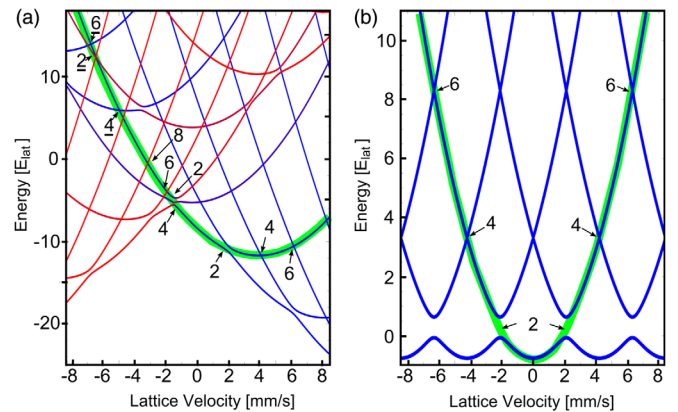

FIG. 2 (color online). Effective band structure as a function of the lattice velocity. The thick green lines indicate the position at which the BEC is placed in the experiments. (a) BEC with spin-orbit coupling and $\hbar\delta = 1.6E_{\mathrm{Ram}}$ as shown in Fig. 3(b). (b) BEC without spin-orbit coupling as in Fig. 4. The numbers in the graphs indicate the order of the associated multiphoton resonances.
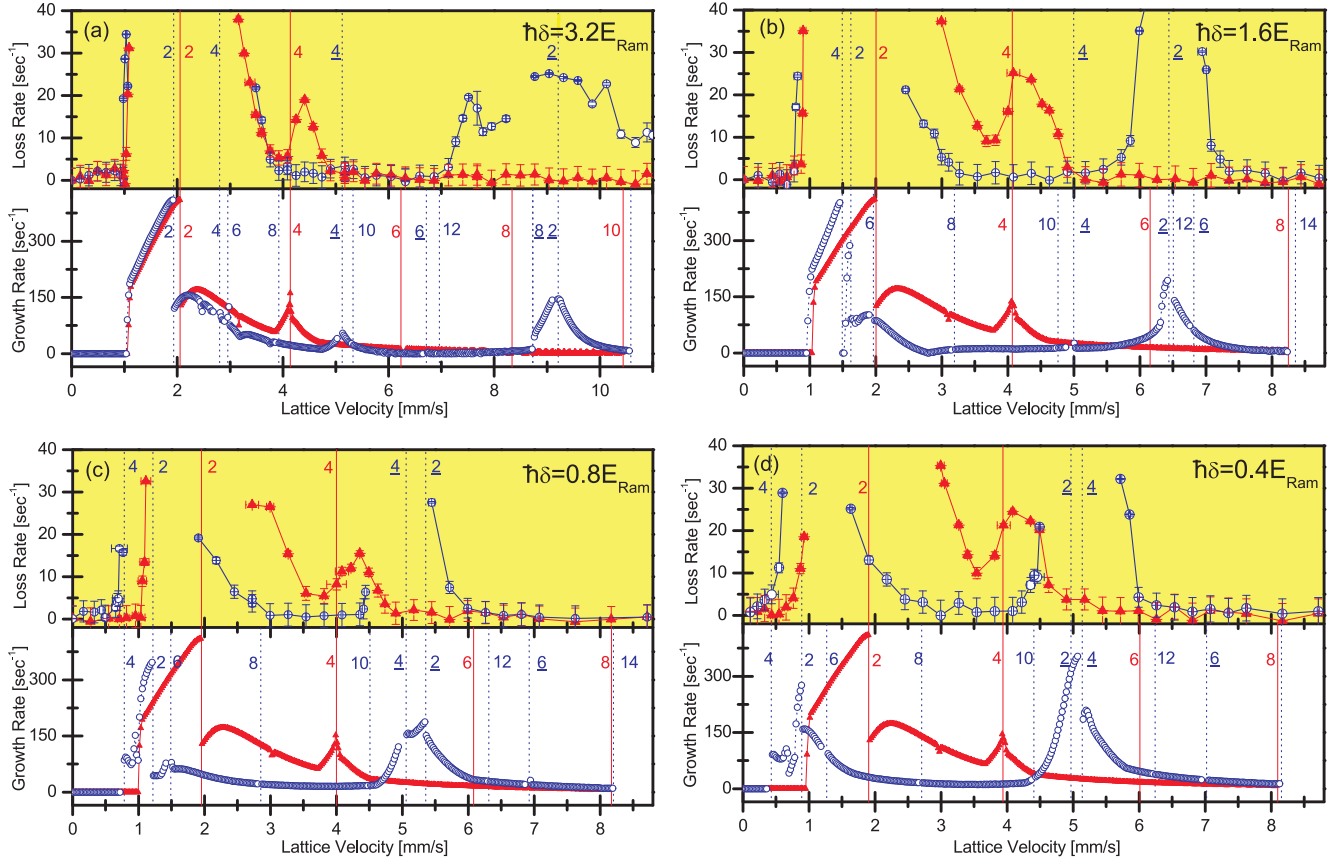
FIG. 3 (color online). Dynamical instability of the spin-orbit-coupled BEC as a function of lattice speed with
(a)–(d) $\hbar\delta/E_{\mathrm{Ram}} = \{3.2, 1.6, 0.8, 0.4\}$, respectively. The strength of the dynamical instability is measured experimentally by the loss
rate of atoms in the BEC (upper panels), while theoretically it is represented by the largest growth rate of Bogoliubov excitations (lower
panels). Each resonance (vertical line) is labeled with the number of photons generating the band edge, with underlined integers
denoting resonances between the upper and lower spin-orbit bands. The solid red triangles (open blue circles) indicate the positive
(negative) direction of the lattice motion.

to the lattice potential, $\bar{H}_{\mathrm{sp}}^M$ is nontrivially different from
H_{SOC} due to the term $\delta + 2m\gamma v/\hbar$, which can be inter-
preted as an effective detuning of the Raman beams. This
term depends on the frame velocity v and signifies the
broken Galilean invariance of the spin-orbit-coupled BEC.
Physically, this arises because the Raman lasers generating
the spin-orbit coupling provide a fixed frame of reference.

In our experiments, we observe the behavior of the BEC
by varying the lattice velocity. An effective dispersion
relation should thus be calculated as a function of the lattice
velocity v. The BEC is initially assumed to be in the ground
state of the spin-orbit-coupled band $E_-(k_z)$ of H_{SOC} with a
finite quasimomentum, k_{min}, which is approximately con-
served when the optical lattice is introduced [31].
Therefore, during the experiment, the quasimomentum
k_{min} is fixed. The effective dispersion, $E^M(k_{\mathrm{min}}, v)$, can
be taken from the Bloch spectrum of H_{sp}^M at k_{min}. The
results are shown in Fig. 2(a) for $\hbar\delta = 1.6E_{\mathrm{Ram}}$,
$\hbar\Omega = 2E_{\mathrm{Ram}}$, and $U_0 = -1.4E_{\mathrm{lat}}$, where $E_{\mathrm{Ram}} = (\hbar k_{\mathrm{Ram}})^2/2m$. An obvious feature of the effective dispersion relation

is its asymmetry with respect to a sign change of the lattice
velocity. The physical origin of this asymmetry is the
breaking of Galilean invariance.

From the effective dispersion, we can trace the location of
the BEC if the lattice velocity varies. When the spin-orbit-
coupled BEC is adiabatically loaded into the translating
lattice, it occupies a state near the lower spin-orbit-coupled
band $E_-^M(k_{\mathrm{min}}, v)$ [thick green line in Fig. 2(a)]. We label the
avoided crossings along the trace by integers $2n$ that indicate
the photon processes involved, $E_-^M(k_{\mathrm{min}}, v) = E_-^M(k_{\mathrm{min}} \pm 2nk_{\mathrm{lat}}, v)$. Resonances occurring between the lower and
upper spin-orbit bands $[E_-^M(k_{\mathrm{min}}, v) = E_+^M(k_{\mathrm{min}} \pm 2nk_{\mathrm{lat}}, v)]$
are denoted by an underlined number $\underline{2n}$. It is interesting to
note that the ordering of the band edges is not straightfor-
ward, and the positions of the band edges are not equally
spaced. The exact ordering and positions strongly depend on
the chosen parameters δ, Ω, and the ratio $k_{\mathrm{lat}}/k_{\mathrm{Ram}}$. For
comparison, Fig. 2(b) presents the analogous band structure
for a BEC in a translating lattice but without spin-orbit
coupling. As is well known in this case, the effective band

structure and the BEC location (thick green line) are symmetric with respect to the direction of motion, the band edges are equally spaced, and the effective dispersion relation recovers the Bloch spectrum.

The avoided crossings of the effective dispersion are experimentally probed by the observation of dynamical instability of the BEC. We measure the loss spectra for the system as a function of the velocity of the optical lattice. Our experiments begin with a nearly pure ^{87}Rb BEC in the ground state in the presence of spin-orbit coupling with $\hbar\Omega = 2E_{Ram}$ before ramping up a translating optical lattice to a lattice depth of $U_0 = -1.4E_{lat}$ [30]. We hold the BEC in the lattice potential for 100 ms, during which excitations caused by instabilities can grow and population is lost from the BEC. The experimental results for the loss rate as a function of the lattice velocity, for four different values of the Raman detuning δ, are plotted in the upper panels of Figs. 3(a)–3(d). In the absence of Galilean invariance, we must differentiate between the two translating directions for the optical lattice. In Fig. 3, we plot negative (positive) velocities in dashed open blue circles (solid red triangles), corresponding to the dashed (solid) arrows in Fig. 1(c). With this convention, a lattice translating in the positive direction couples to states that resemble free particles, while a lattice translating in the negative direction couples to states that are strongly modified by the spin-orbit coupling. For comparison, we have also performed these measurements without spin-orbit coupling (see Fig. 4) and for this case, find agreement with prior experimental work [27].

We model our experiment using the Bogoliubov–de Gennes (BdG) equations based on a one-dimensional mean-field description of a homogeneous BEC [30]. We identify the quasiparticle mode with the largest imaginary part of the energy, corresponding to the largest initial growth rate, and plot this rate as a function of velocity in the lower panels of Figs. 3(a)–3(d). The theoretical results provide a good understanding of the experimental measurements [30]. While the theoretically calculated growth rates are different quantities than the experimental loss rates presented in the upper panels of Fig. 3, they have previously been found to be a reasonable indication of the strength of dynamical instability [27]. Both the experimental data and the numerical results demonstrate that the critical speed for the onset of the dynamical instability is different for the two directions of motions. This is particularly evident in the experimental and numerical results for the smaller detunings of $\hbar\delta = 0.8E_{Ram}$ and $\hbar\delta = 0.4E_{Ram}$ in Figs. 3(c) and 3(d) near $v = \pm 0.5$ mm/s, where the critical velocity is smaller for the negative direction. Above the critical velocity, the dynamical instability is most significant in the vicinity of the band edges. Loss occurs in all higher bands as well, but the loss rate in higher bands is significantly reduced.

The dynamical stability of the BEC is also quite different for the two directions of motion. In Figs. 3(a)–3(d), the
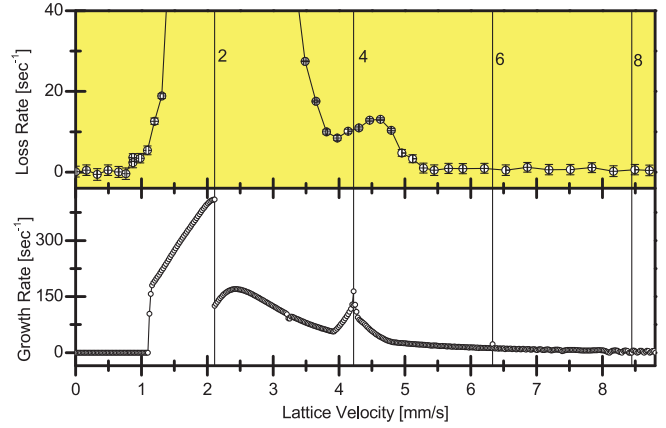

FIG. 4 (color online). Dynamical instability of the BEC without spin-orbit coupling as a function of lattice velocity. The strength of the dynamical instability is measured experimentally by the loss rate of atoms in the BEC (upper panels), while theoretically, it is represented by the largest growth rate of any Bogoliubov excitation (lower panels). Each resonance (vertical line) is labeled with the number of photons generating the band edge.

behavior of the loss and growth rates for the positive direction of motion (red solid triangles) is very similar to that of the case without spin-orbit coupling shown in Fig. 4. However, in the negative direction of motion (blue open circles), the behavior is strongly modified. For example, in Fig. 3(a) for $\hbar\delta = 3.2E_{Ram}$, a pronounced additional loss feature appears centered around $v = 9$ mm/s, shifting to smaller velocities for smaller δ in Figs. 3(b)–3(d). This feature is caused by the two-photon resonance $\underline{2}$ between $E_-^M(k_{min}, v)$ and $E_+^M(k_{min} - 2k_{lat}, v)$ (i.e., the lattice resonance between the lower and upper spin-orbit bands). For comparison, the large loss feature near $v = 2$ mm/s is due to the two-photon resonance within the lowest spin-orbit band. Even though both of these loss features arise from two-photon couplings, the $\underline{2}$ feature is weaker. This is in part due to the reduced overlap of the spin composition between $E_-^M(k_{min}, v)$ and $E_+^M(k_{min} - 2k_{lat}, v)$. For the positive direction of motion of the lattice in Figs. 3(a)–3(d), the $\underline{2}$ resonance between $E_-^M(k_{min}, v)$ and $E_+^M(k_{min} + 2k_{lat}, v)$ occurring at large velocity is suppressed by the small overlap in spin composition for our chosen parameters. For example, with $\hbar\delta = 1.6E_{Ram}$, such a resonance occurs at $v = 21.6$ mm/s but the modification to the Bloch spectrum is negligible. Another loss feature near $v = 4.5$ mm/s in Fig. 3(a) in the positive direction corresponds to the four-photon resonance and is shifted to smaller velocities in the negative direction. In the experimental results for the negative direction, it cannot be differentiated from the dominant 2 band edge and is diminished due to the smaller overlap of the spin compositions.

In conclusion, we have studied the rich dispersion relation of a spin-orbit-coupled BEC in a weak optical lattice by probing the losses of the system as a function of

lattice velocity. Our experiment provides a direct observation of the breaking of Galilean invariance in the presence of spin-orbit coupling. Our spin-orbit-coupled lattice BEC affords an important platform to experimentally investigate the effect of spin-orbit coupling for the superfluid–to–Mott-insulator transition and the magnetic physics in spin-orbit-coupled Mott-insulator phases [32–34].

*engels@wsu.edu

[1] N. Nagaosa, J. Sinova, S. Onoda, A. H. MacDonald, and N. P. Ong, Rev. Mod. Phys. **82**, 1539 (2010).

[2] M. W. Haverkort, I. S. Elfimov, L. H. Tjeng, G. A. Sawatzky, and A. Damascelli, Phys. Rev. Lett. **101**, 026406 (2008).

[3] C. L. Kane and E. J. Mele, Phys. Rev. Lett. **95**, 226801 (2005).

[4] L. Fu, C. L. Kane, and E. J. Mele, Phys. Rev. Lett. **98**, 106803 (2007).

[5] M. Z. Hasan and C. L. Kane, Rev. Mod. Phys. **82**, 3045 (2010).

[6] X.-L. Qi and S.-C. Zhang, Rev. Mod. Phys. **83**, 1057 (2011).

[7] G. Jackeli and G. Khaliullin, Phys. Rev. Lett. **102**, 017205 (2009).

[8] G. Chen, R. Pereira, and L. Balents, Phys. Rev. B **82**, 174440 (2010).

[9] Y.-J. Lin, K. Jiménez-García, and I. B. Spielman, Nature (London) **471**, 83 (2011).

[10] Z. Fu, P. Wang, S. Chai, L. Huang, and J. Zhang, Phys. Rev. A **84**, 043609 (2011).

[11] J.-Y. Zhang, S.-C. Ji, Z. Chen, L. Zhang, Z.-D. Du, B. Yan, G.-S. Pan, B. Zhao, Y.-J. Deng, H. Zhai, S. Chen, and J.-W. Pan, Phys. Rev. Lett. **109**, 115301 (2012).

[12] C. Qu, C. Hamner, M. Gong, C. Zhang, and P. Engels, Phys. Rev. A **88**, 021604(R) (2013).

[13] C. Hamner, C. Qu, Y. Zhang, J. Chang, M. Gong, C. Zhang, and P. Engels, Nat. Commun. **5**, 4023 (2014).

[14] A. J. Olson, S.-J. Wang, R. J. Niffenegger, C.-H. Li, C. H. Greene, and Y. P. Chen, Phys. Rev. A **90**, 013616 (2014).

[15] J. Dalibard, F. Gerbier, G. Juzeliūnas, and P. Öhberg, Rev. Mod. Phys. **83**, 1523 (2011).

[16] V. Galitski and I. B. Spielman, Nature (London) **494**, 49 (2013).

[17] N. Goldman, G. Juzeliūnas, P. Öhberg, and I. B. Spielman, Rep. Prog. Phys. **77**, 126401 (2014).

[18] H. Zhai, arXiv:1403.8021.

[19] J. Higbie and D. M. Stamper-Kurn, Phys. Rev. Lett. **88**, 090401 (2002).

[20] Y. Li, G. I. Martone, and S. Stringari, arXiv:1410.5526.

[21] Y. Xu and C. Zhang, Int. J. Mod. Phys. B **29**, 1530001 (2015).

[22] Y. Zhang and C. Zhang, Phys. Rev. A **87**, 023611 (2013).

[23] Q. Zhu, C. Zhang, and B. Wu, Europhys. Lett. **100**, 50003 (2012).

[24] M. Krämer, C. Menotti, L. Pitaevskii, and S. Stringari, Eur. Phys. J. D **27**, 247 (2003).

[25] B. Wu and Q. Niu, Phys. Rev. A **64**, 061603 (2001).

[26] A. Smerzi, A. Trombettoni, P. G. Kevrekidis, and A. R. Bishop, Phys. Rev. Lett. **89**, 170402 (2002).

[27] L. Fallani, L. De Sarlo, J. E. Lye, M. Modugno, R. Saers, C. Fort, and M. Inguscio, Phys. Rev. Lett. **93**, 140406 (2004).

[28] M. Modugno, C. Tozzo, and F. Dalfovo, Phys. Rev. A **70**, 043625 (2004).

[29] T. Ozawa, L. P. Pitaevskii, and S. Stringari, Phys. Rev. A **87**, 063610 (2013).

[30] See Supplemental Material at http://link.aps.org/supplemental/10.1103/PhysRevLett.114.070401 for a detailed description of the theoretical stability analysis, further details of the experimental methods and considerations, and visualization of the band structure in terms of the effective detuning.

[31] P. Cladé, S. Guellati-Khélifa, F. Nez, and F. Biraben, Phys. Rev. Lett. **102**, 240402 (2009).

[32] Z. Cai, X. Zhou, and C. Wu, Phys. Rev. A **85**, 061605(R) (2012).

[33] W. S. Cole, S. Zhang, A. Paramekanti, and N. Trivedi, Phys. Rev. Lett. **109**, 085302 (2012).

[34] J. Radić, A. Di Ciolo, K. Sun, and V. Galitski, Phys. Rev. Lett. **109**, 085303 (2012).